NUMERICAL STUDY OF PRESSURE DROP AND FLUID FRICTION IN LAMINAR FLOW RECTANGULAR MICRO-CHANNELS

Hayder Mohammed Hasan
Shatra Technical Institute, Machines and Equipment department/ Automotive Branch

ABSTRACT

An incompressible three dimensional continuity and Navier-Stokes (momentum equations) equations are numerically solved to obtain the pressure drop and fluid friction in laminar steady state micro-channel flow of water. The governing equations are solved by using SIMPLE algorithm with finite volume method and FORTRAN code to obtain pressure field in rectangular micro-channel and then from the pressure field both friction factor *f* and friction constant *Cf* are obtained.

The results showed that the factors affecting the pressure drop, friction factor *f* and friction constant *Cf* are; channel length *L*, Reynolds number Re, aspect ratio α, channel volume V_{ch} and hydraulic diameter D_h. Increasing of channel length *L* leads to increase each pressure drop, *f* and *Cf*. On other hand, increasing of Re leads to increase pressure drop and decrease the *f*, while the *Cf* increase with low value of Re (Re less than 50) and then nearby with approximately constant value. Moreover, increasing of α, V_{ch} and D_h each separately leads to decrease pressure drop and increase both *f* and *Cf*.

دراسة عددية لهبوط الضغط واحتكاك المائع في جريان طباقي لقنوات مايكروية مربعة الشكل

م.م حيدر محمد حسن ، المعهد التقني في الشطرة/ قسم المكائن والمعدات/ السيارات

الخلاصة

معادلة الاستمرارية (continuity equation) ومعادلات الزخم (momentum equations) تم حلها بطريقة عددية لإيجاد هبوط الضغط (pressure drop) ومعامل الاحتكاك (friction factor *f*) وثابت الاحتكاك (friction constant *Cf*) لجريان طباقي ثلاثي الأبعاد في حالة الاستقرار ولا انضغاطي لماء يجري في قنوات مايكروية مربعة الشكل. تم حل معادلة الاستمرارية ومعادلات الزخم باستخدام طريقة (SIMPLE method) وقد تم تحويل المعادلات الحاكمة إلى الشكل العددي باستخدام طريقة الحجوم المحددة (finite volume method) وباستخدام لغة فورتران (FORTRAN) تم حل هذه المعادلات. بهذه الطريقة تم إيجاد توزيع الضغط في المائع, ومن خلال إيجاد توزيع الضغط يمكن ايجاد معامل الاحتكاك وثابت الاحتكاك.

من خلال ملاحظة نتائج الحل العددي, تبين بأن هنالك مجموعة من العوامل التي تؤثر على هبوط الضغط ومعامل الاحتكاك وثابت الاحتكاك وهي: طول القنوات (channel length *L*) وعدد رينولدز(Reynolds number Re) ونسبة الارتفاع الى العرض (aspect ratio α) وحجم القنوات (channel volume V_{ch}) والقطر المكافئ (hydraulic diameter D_h). عند زيادة *L* فأن كل من هبوط الضغط ومعامل وثابت الاحتكاك يزداد وعند زيادة Re يزداد هبوط الضغط ويقل معامل الاحتكاك بينما ثابت الاحتكاك يزداد عند قيم صغيرة لعدد رينولدز (Re<50) ومن ثم يبدو ثابتاً بعد ذلك وعند زيادة α و V_{ch} و D_h كل على حدة يقل هبوط الضغط ويزداد معامل وثابت الاحتكاك.

KEYWORDS: laminar flow, rectangular micro-channel, numerical solution, pressure drop, friction factor and friction constant

NOMENCLACHRE

English symbols

D_h	hydraulic diameter . .. . *m*
H_{ch}	channel height . . . . . *m*
L	channel length . .. . *m*
p	pressure . . .. *Pa*
Δp	pressure drop . . . . *Pa*
u	fluid *x*-component velocity . . . *m/s*
v	fluid *y*-component velocity . . . . *m/s*
w	fluid *z*-component velocity ... .. .*m/s*
W_{ch}	channel width . . . .*m*
x	axial coordinate . . . .*m*
y	horizontal coordinate . . . . . *m*
z	vertical coordinate . . . . . .*m*

Greek symbols

μ	dynamic viscosity . . . . *Pa/s*
ρ	density . . . . . *kg/m*^{3}

Dimensionless groups

$Cf = f\,\mathrm{Re}$	friction constant
$f = \frac{\Delta p D_h}{2L\rho u_{in}^2}$	friction factor
$\mathrm{Re} = \rho u_{in} D_h / \mu$	Reynolds number
$\alpha = H_{ch} / W_{ch}$	aspect ratio

Subscripts

ch	channel
in	inlet
m	mean

1. Introduction

The fast development of high density of very large scale integration (VLSI) microelectronic circuit required more and more effective ways of cooling the microchips. In principle the higher level of integrity (responsible for the computer processor unit CPU speed) the more heat is released as shown in Fig. 1 [1]. The tendency presented here makes it clear that further progress in VLSI systems development is limited by the capabilities in heat removal from microprocessors. As a possible solution micro-channel based circuits with liquid cooling media can be employed as providing very high heat transfer coefficient. Although such systems are being already constructed (see sample design in Fig. 2) their performance is still far from being quite satisfactory and a lot of research efforts have to be done to solve the existing problems [2]. In micro-channel flow, the Knudsen number is a measure of the degree of the rarefaction which is defined as the ratio of mean free path to the characteristic length scale of the system. The flow regimes could be classified as: continuum regime (Kn<0.001), slip flow regime (0.001<Kn<0.1), transient regime (0.1<Kn<10) and free molecular regime (Kn>10). In order to simulate the no slip flow regime, the Knudsen number is Kn<0.001 [3].

The main advantage of small channels is their high cooling performance. It may be even up to 60 times higher when used in heat exchangers than the corresponding values of micro-channels leads, however, to significantly increased flow resistance which is a serious drawback of this technology [2]. Several early studies provided results on the friction factor and pressure drop, Wu and Little [4] investigated the friction factor in micro-channels (etched in silicon and glass) with hydraulic diameters ranging from 55.81 to 83.08μm. They found that the friction factor up to 30% higher than the value predicted for the circular pipe on the basis of conventional law. Shah and London [5] compiled a comprehensive solution for laminar forced convection flow heat transfer in wide range of ducts sizes and shapes. Muzychka [6] developed an analytical and experimental study for the fluid friction and heat transfer for wide range of channels geometries. He showed that the square root of cross-section flow area as characteristic length provide better correlations for wide range of the ducts, that could be achieved by the hydraulic diameter. Harley and Bau [7] measured the friction factor in micro-channels. They concluded that the product *f* Re is higher than the classical value. Adams et al. [8]

2. Analysis

In this section the hydrodynamic characteristics of rectangular micro-channel flow is investigated numerically and the parameters that affect its performance are examined. This investigation done by solving the three dimensional developing laminar flow. Schematic structure of network is shown in Fig. 3 (a) which may be heat exchanger or heat sink, the micro-channels system was supplied with the circulating working liquid by the external closed-loop circuit. The fluid is distributed among the micro-channels through the inlet channels termed as distributor and then collected by the collector. The micro-channels are of rectangular cross-section as shown in Fig. 3 (b) which represents a complete assembly and gives an adequate indication about its micro-channel flow due to symmetry between channels rows; so that we will consider an individual unite.

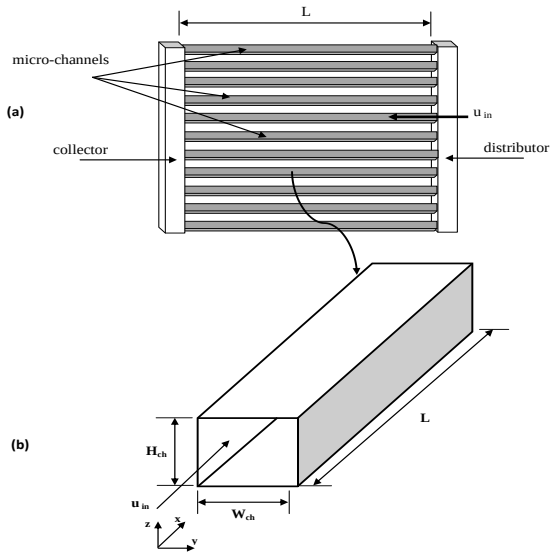

Fig. 3. Schematic model of micro-channel.

However, the governing equations for the present model are based on the following physical and geometrical assumptions:

- Three dimensional steady incompressible laminar flow along the length of channel.
- The Knudsen number is small enough so that, the fluid is a continuous medium (no slip).
- Newtonian fluid with constant properties; in this case the water is used as working fluid.
- The pressure gradient is in axial direction only.
- Heat transfer is not effected on the flow.

The governing equations in general form for present model consist of continuity and momentum equations (Navier-stokes equations) and they are [13]:

$$\nabla . \vec{V} = 0 \tag{1}$$

$$\rho (\vec{V} . \nabla \vec{V}) = -\nabla P + \mu \nabla^2 \vec{V} \tag{2}$$

where $\vec{V}$ represents the velocity vector. The governing equations and its boundary conditions can be written as
continuity equation

$$\frac{\partial u}{\partial x} + \frac{\partial v}{\partial y} + \frac{\partial w}{\partial z} = 0 \tag{3}$$

momentum equations (Navier-stokes equations):

$$\rho\left(u\frac{\partial u}{\partial x} + v\frac{\partial u}{\partial y} + w\frac{\partial u}{\partial z} \right) = -\frac{\partial P}{\partial x} + \mu\left(\frac{\partial^2 u}{\partial x^2} + \frac{\partial^2 u}{\partial y^2} + \frac{\partial^2 u}{\partial z^2} \right) \tag{4}$$

$$\rho\left(u\frac{\partial v}{\partial x} + v\frac{\partial v}{\partial y} + w\frac{\partial v}{\partial z} \right) = \mu\left(\frac{\partial^2 v}{\partial x^2} + \frac{\partial^2 v}{\partial y^2} + \frac{\partial^2 v}{\partial z^2} \right) \tag{5}$$

$$\rho\left(u\frac{\partial w}{\partial x} + v\frac{\partial w}{\partial y} + w\frac{\partial w}{\partial z} \right) = \mu\left(\frac{\partial^2 w}{\partial x^2} + \frac{\partial^2 w}{\partial y^2} + \frac{\partial^2 w}{\partial z^2} \right) \tag{6}$$

The boundary conditions are:

$$At \quad x = 0$$

$$u = u_{in} \, , v = w = 0$$

$$At \quad x = L$$

$$\frac{\partial u}{\partial x} = \frac{\partial v}{\partial x} = \frac{\partial w}{\partial x} = 0$$

$$At \quad y = 0 \; and \quad y = W_{ch}$$

$$u = v = w = 0$$

$$At \quad z = 0 \; and \; z = H_{ch}$$

$$u = v = w = 0$$

the above governing equations are solved using FORTRAN code as shown in the next section and then the pressure field can be determined.

3. Numerical Solution

The above equations are discretized into the numerical form using the finite volume method with staggered grid arrangement. Finite volume methods are applied to the integral form of the governing equations over the control volume (cell) as shown in Fig. 4. A cell containing node ***P*** has four neighbouring nodes identified as west, east, south and north nodes ***(W, E, S, N).*** The notation, ***w, e, s and n*** are used to refer to the west, east, south and north cell faces respectively. This technique can be extended to three dimensional control volume as can be seen from the Fig. 5 to solve pressure-velocity coupling which associated with present work by pressure-correction method with SIMPLE algorithm as listed in [14].

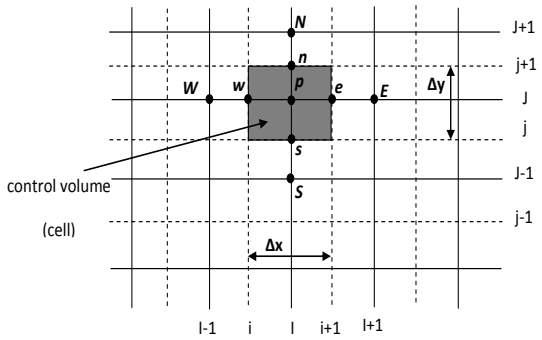

Fig. 4. Two dimensional control volume around node *P* [14].

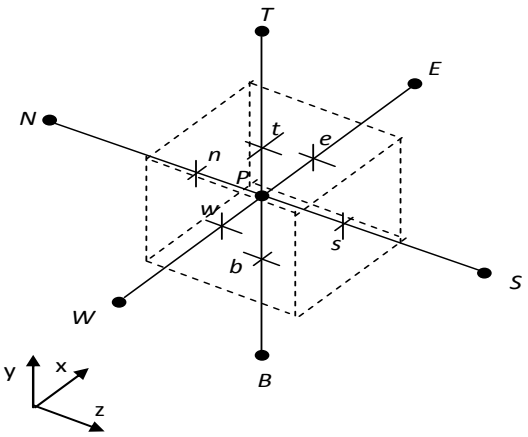

Fig. 5. Three dimensional control volume around node *P* [14].

The solution was treated as converged when the level of residual was lower than 10^{-5}. The grid quality was checked by performing grid independence tests of the solution in terms of the pressure drop across the system. The consecutive calculations were performed for grid 100, 50 and 50 in x, y and z directions respectively and the greatest differences found were lower than 3%.

The first step in the numerical approach is the grid generation and then discretisation the governing equations by integration them over the special control volume (cell). The discretisation of *u*-component in equation (4) by using finite volume method as the following [14]:

$$\rho \int_{cv} \left[\frac{\partial}{\partial x}(uu) + \frac{\partial}{\partial y}(vu) + \frac{\partial}{\partial z}(wu) \right] dv = \int_{cv} \left[-\frac{\partial p}{\partial x} + \mu \left(\frac{\partial^2 u}{\partial x} + \frac{\partial^2 u}{\partial y} + \frac{\partial^2 u}{\partial z} \right) \right] dv \tag{7}$$

where *dv* represent the control volume. Distribution the integral form on each term in equation (7) gives

$$\int_w^e \frac{\partial}{\partial x}(\rho uu)dv + \int_s^n \frac{\partial}{\partial y}(\rho vu)dv + \int_b^t \frac{\partial}{\partial z}(\rho wu)dv = -\int_w^e \frac{\partial p}{\partial x} dv + \left(\mu \int_w^e \frac{\partial^2 u}{\partial x} dv + \mu \int_s^n \frac{\partial^2 u}{\partial y} dv + \mu \int_b^t \frac{\partial^2 u}{\partial z} dv \right) \tag{8}$$

result of integration is

$$\left(a_W + a_E + a_S + a_N + a_B + a_T + \Delta F\right)u_{(P)} = -\left(p_{(e)} - p_{(w)}\right) + \begin{pmatrix} a_W u_W + a_E u_E + a_S u_S + \\ a_N u_N + a_B u_B + a_T u_T \end{pmatrix} \quad (9)$$

where $\Delta F = \left(F_e - F_w\right) + \left(F_n - F_s\right) + \left(F_t - F_b\right)$ and $F=\rho u$, where u the average velocity in each cell face.

Also, $a_{w,s,b} = D + F/2$ and $a_{e,n,t} = D - F/2$ where $D = \mu/\delta$, the term δ represent grid step in each direction.

Again, equation (9) reduced to

$$a_P\, u_{(P)} = -\left(p_{(e)} - p_{(w)}\right) + a_W u_W + a_E u_E + a_S u_S + a_N u_N + a_B u_B + a_T u_T \quad (10)$$

Equation (10) represent the discretisation equation where

$$a_P = a_W + a_E + a_S + a_N + a_B + a_T + \Delta F$$

Similar procedures to obtain the discretisation equation for v and w velocity components.

The above equations solved by SIMPLE algorithm. Discretized u-component equation (10) is written in the following form [14]

$$a_{(i,J,K)}u_{(i,J,K)} = \sum a_{nb}u_{nb} + \left(p_{(I-1)} - p_{(I)}\right) \quad (11)$$

where, $\sum a_{nb}u_{nb}$ is the summation of neighbouring components for u-component. The values of coefficients $a_{(i,J,K)}$ and a_{nb} in equation (11) are calculated by using the central differencing method. However, to initiate the SIMPLE calculation process a pressure field p^* is guessed. Discretised momentum equation (10) is solved using the guessed pressure field to yield velocity component u^* as follows

$$a_{(i,J,K)}u^*_{(i,J,K)} = \sum a_{nb}u^*_{nb} + \left(p^*_{(I-1)} - p^*_{(I)}\right) \quad (12)$$

Now we defined the correction p'' as the difference between the correct pressure field p and the guessed pressure field p^*, so that

$$p = p^* + p'' \quad (13)$$

Similarly we defined velocity correction u'' to relate the correct velocity u to the guessed velocity solution u^*

$$u = u^* + u'' \quad (14)$$

Subtraction of equation (12) from equation (11) gives

$$a_{(i,J,K)}\left(u_{(i,J,K)} - u^*_{(i,J,K)}\right) = \sum a_{nb}\left(u_{nb} - u^*_{nb}\right) + \begin{bmatrix} \left(p_{(I-1)} - p^*_{(I-1)}\right) \\ -\left(p_{(I)} - p^*_{(I)}\right) \end{bmatrix} \quad (15)$$

Using correction formulae (13) and (14), the equation (15) may be rewritten as follows

$$a_{(i,J,K)}u''_{(i,J,K)} = \sum a_{nb}u''_{nb} + \begin{pmatrix} p''_{(I-1)} \\ -\,p''_{(I)} \end{pmatrix} \quad (16)$$

At this point an approximation is introduced: $\sum a_{nb}u''_{nb}$ is dropped to simplify equation (16) for velocity correction. Omission of that term is the main approximation of the SIMPLE. We obtain

$$u''_{(i,J,K)} = d_{(i,J,K)}\left(p''_{(I-1)} - p''_{(I)}\right) \quad (17)$$

where $d_{(i,J,K)} = 1/a_{(i,J,K)}$. Equation (17) describe the correction to be applied to u-component through equation (14), which gives

$$u_{(i,J,K)} = u^*_{(i,J,K)} + d_{(i,J,K)}\begin{pmatrix} p''_{(I-1)} \\ -\,p''_{(I)} \end{pmatrix} \quad (18)$$

Similar expression exist for $u_{(i+1,J,K)}$

$$u_{(i+1,J,K)} = u^*_{(i+1,J,K)} + d_{(i+1,J,K)}\begin{pmatrix} p''_{(I)} \\ -\,p''_{(I+1)} \end{pmatrix} \quad (19)$$

where $d_{(i+1,J,K)} = 1/a_{(i+1,J,K)}$.

The SIMPLE algorithm gives a method of calculating pressure and velocity. The method is iterative and when other scalars like present problem are coupled to the momentum equations, the calculations needs to be done sequentially [14]. The sequence of operations in a FORTRAN procedure which employs the SIMPLE algorithm is given in Fig. 6 where

$$b_{(I,J,K)} = \left(u^*_{(i,J,K)} - u^*_{(i+1,J,K)}\right) + \left(v_{(I,j,K)} - v_{(I,j+1,K)}\right) + \begin{pmatrix} w_{(I,J,k)} \\ -\,w_{(I,J,k+1)} \end{pmatrix} \quad (20)$$

In this Fig. the correction method is used for *u*-component only because the pressure-velocity coupling occur hear, but for *v* and *w* component the pressure gradient is neglected therefore no coupling and the velocities obtained without correction.

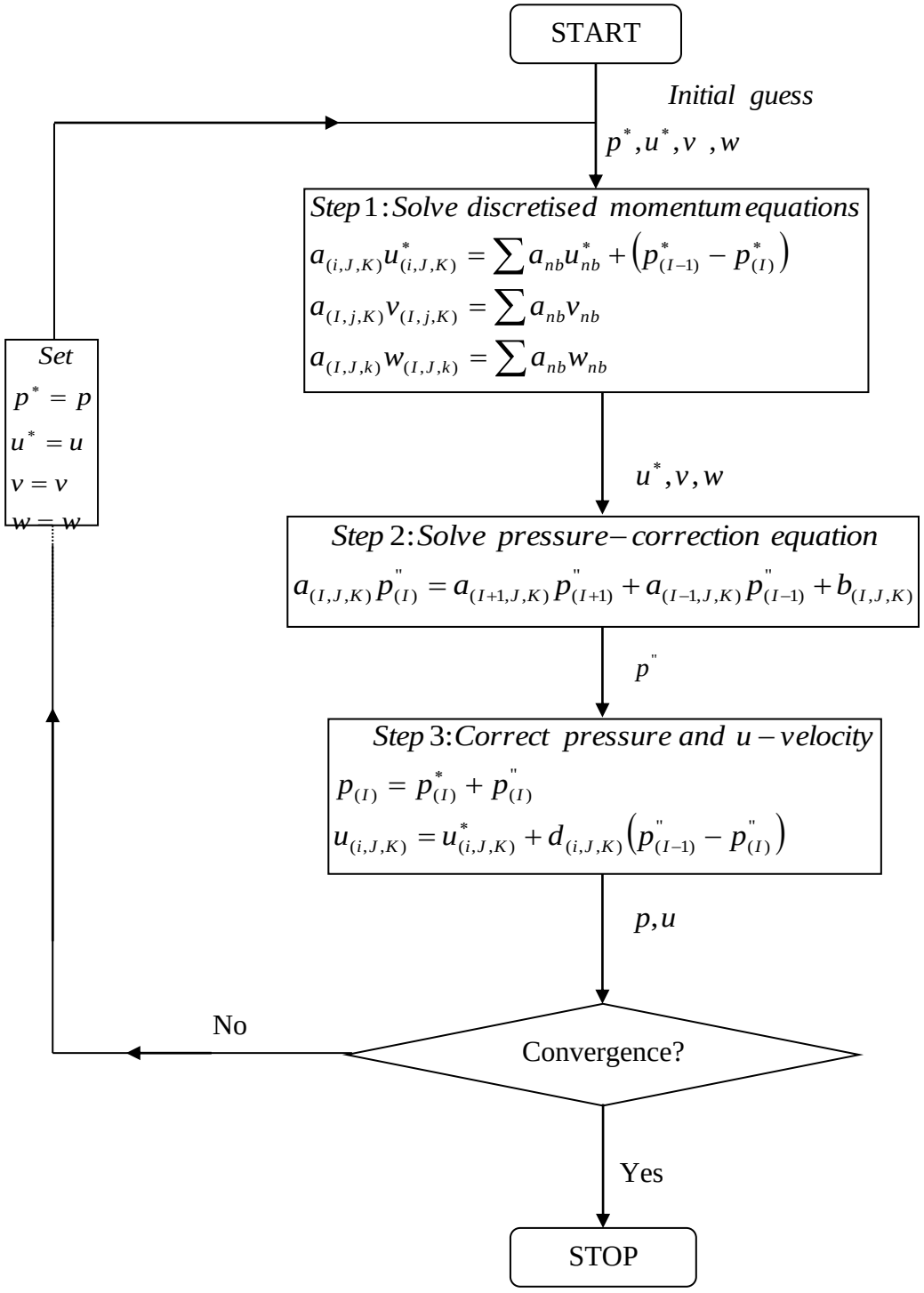

Fig. 6. The SIMPLE algorithm.

4. Results

The study investigates the effects of various parameters such channel length L, Reynolds number Re, aspect ratio α, channel volume V_{ch} and hydraulic diameter D_h on pressure drop, friction factor f where, $f = \frac{\Delta p D_h}{2L\rho u_{in}^2}$ and friction constant Cf where $Cf = fRe$. The results will be involving the effect of each parameter as follows.

Figs. 7-9 indicate the variation of pressure drop, friction factor f and friction constant Cf with channel length L which denoted in the Figs. by variable length x for all channel volume, Reynolds number and aspect ratio. Fig. 7 shows the pressure drop increases with L this due to the fluid inters the channels need more power to flow in long channels, this power reflect in increasing of pressure. In other Figs. the f and Cf also increases with L this due to increasing fluid friction in the channels because the fluid travel longer distance in long channels.

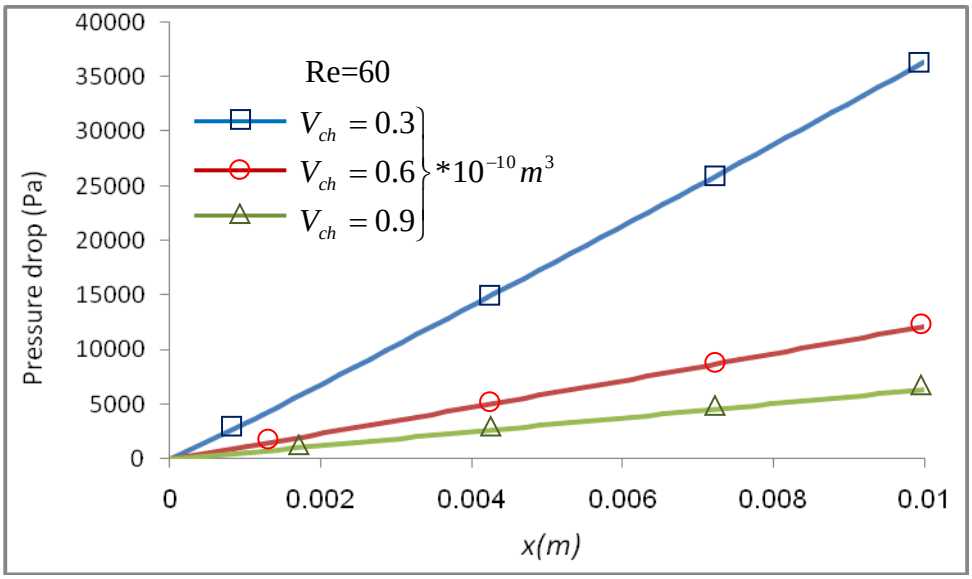

Fig.7. Variation of pressure drop with channel length for different channel volume.

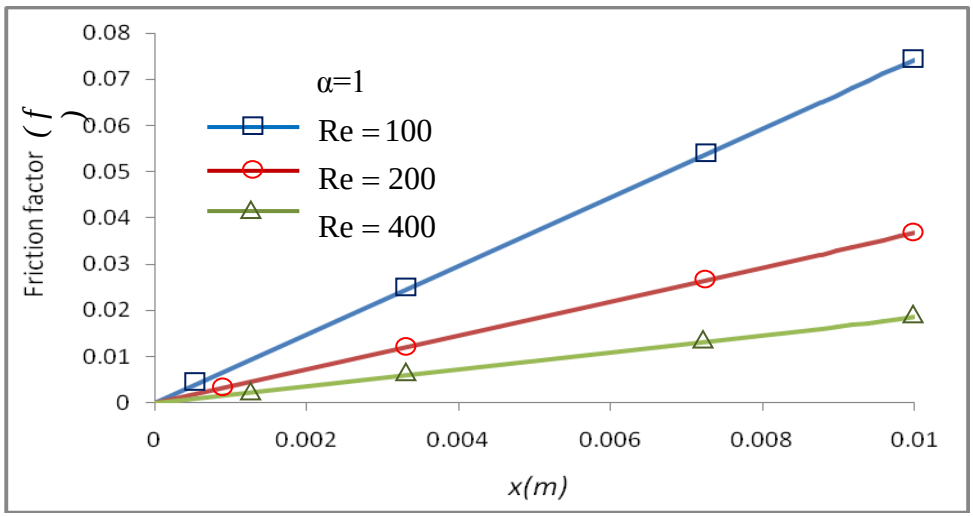

Fig.8. Variation of friction factor with channel length for different Reynolds number.

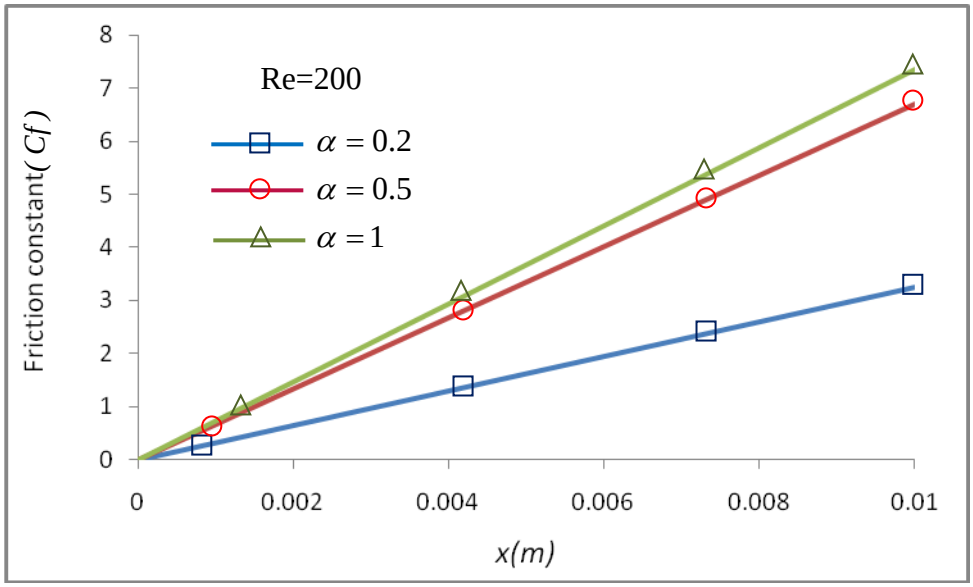

Fig .9. Variation of friction constant with channel length for different aspect ratio.

Fig. 10 and Fig. 11 show the variation of the pressure drop with Reynolds number Re for different values of aspect ratio and channel volumes. The Figs. illustrate that the pressure drop increases with Re due to increase the velocity of fluid and then amount of flow rate inters the channels increase. Also, the Figs. show that pressure drop increases with decreasing channel volume V_{ch} and aspect ratio α due to the velocity of fluid inters the channels increase in this case.

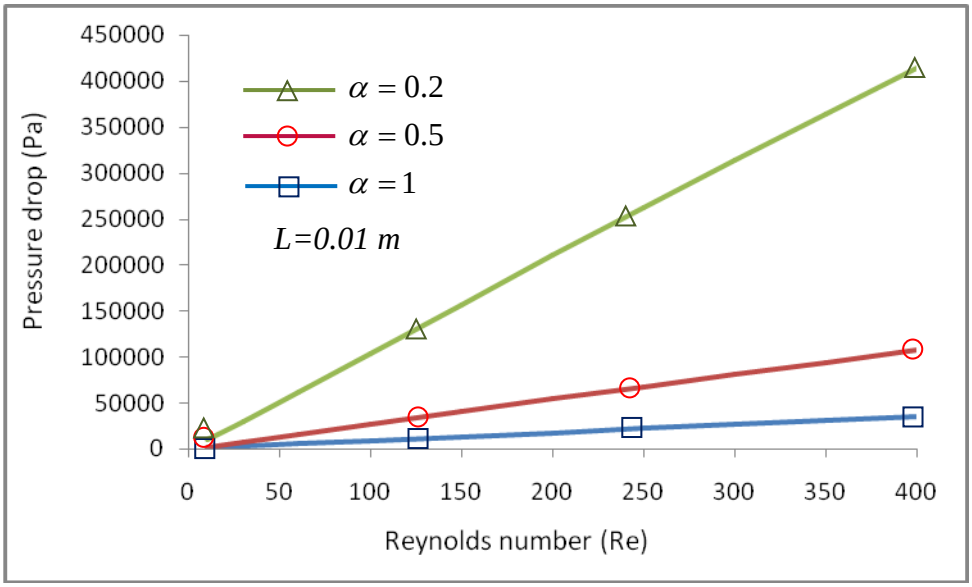

Fig.10. Variation of pressure drop with Reynolds number for different values of aspect ratio.

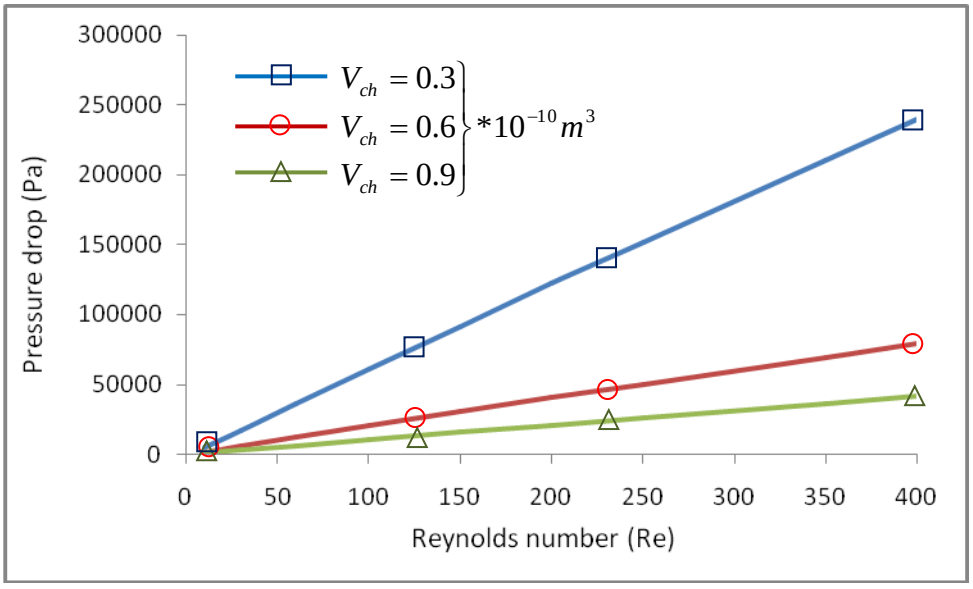

Fig.11. Variation of pressure drop with Reynolds number for different channel volumes.

Fig. 12 and Fig. 13 illustrate the variation of the friction factor f with Reynolds number Re for different values of aspect ratio and channel volumes. The Figs. show that the friction factor f decreases with Re due to increase in the fluid velocity and then fluid friction decrease because $f = \frac{\Delta p D_h}{2L\rho u_{in}^2}$. Also, the Figs. shows that f increase with increase the aspect ratio α and channel volume V_{ch} due to decrease the fluid velocity in the channels with increase of α and V_{ch}.

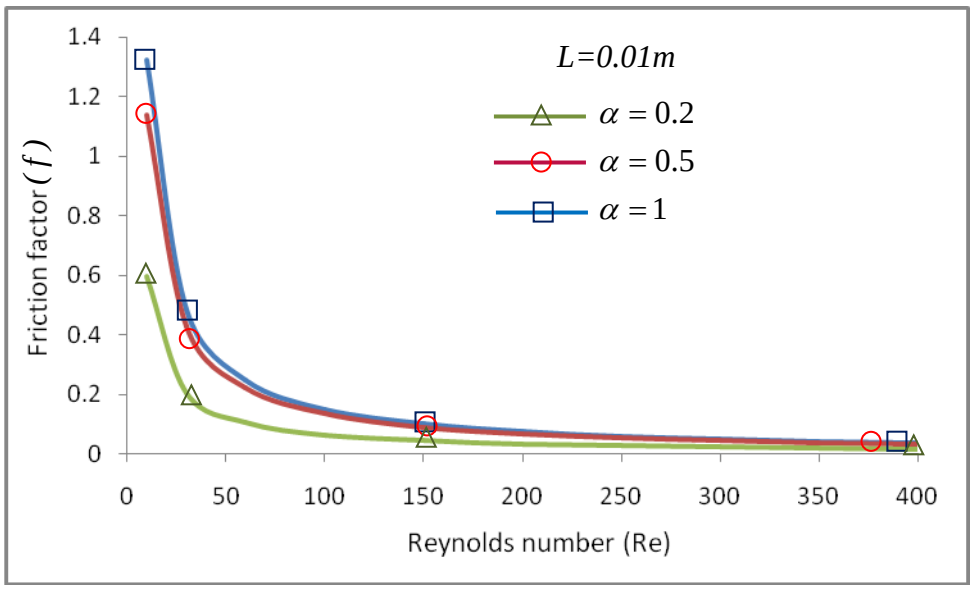

Fig.12. Variation of friction factor with Reynolds number for different values of aspect ratio.

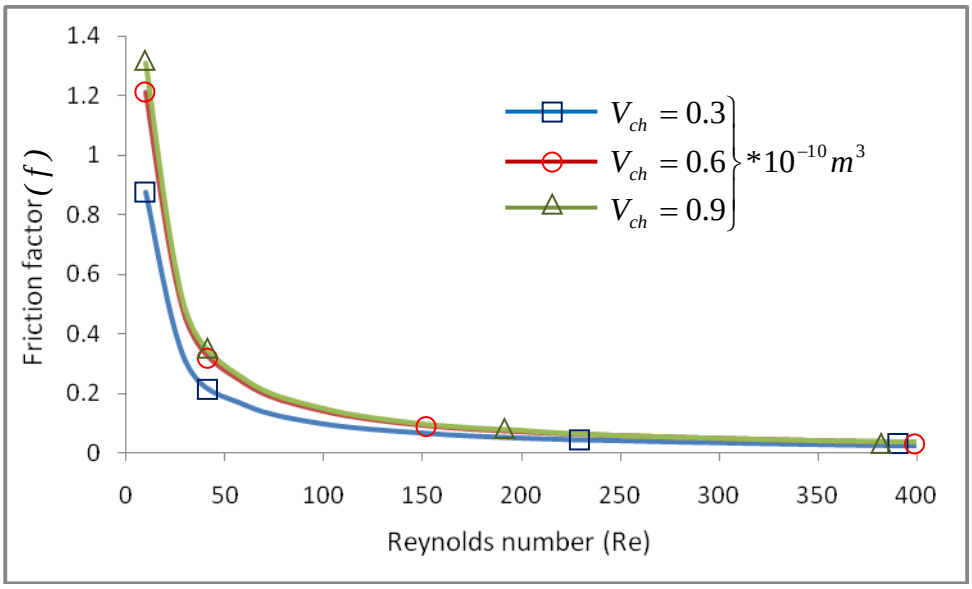

Fig.13. Variation of friction factor with Reynolds number for different channel volume.

Fig. 14 and Fig. 15 indicate the variation of the friction constant *Cf* with Reynolds number Re for different aspect ratio and channel volume. The Figs. show that the *Cf* increases with Re at low values (Re less than 50) and then nearby approximately with constant value because the friction factor *f* is high at low Re due to decreasing of fluid velocity and then decreases rapidly with Re as shown in previous two Figs. Also, the Figs. show that *Cf* increase with increase the aspect ratio α and channel volume V_{ch} due to the *f* increases with α and V_{ch}.

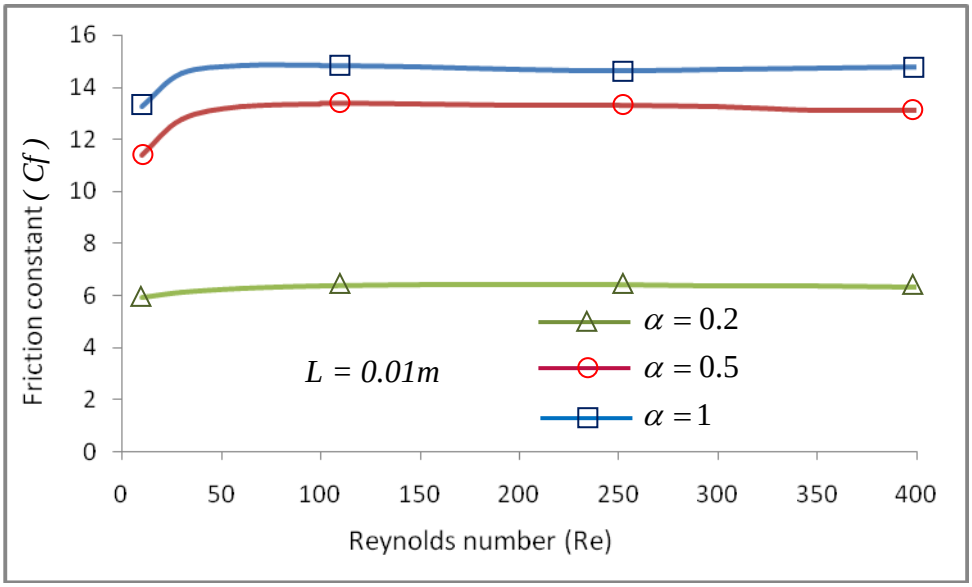

Fig.14. Variation of friction constant with Reynolds number for different aspect ratio.

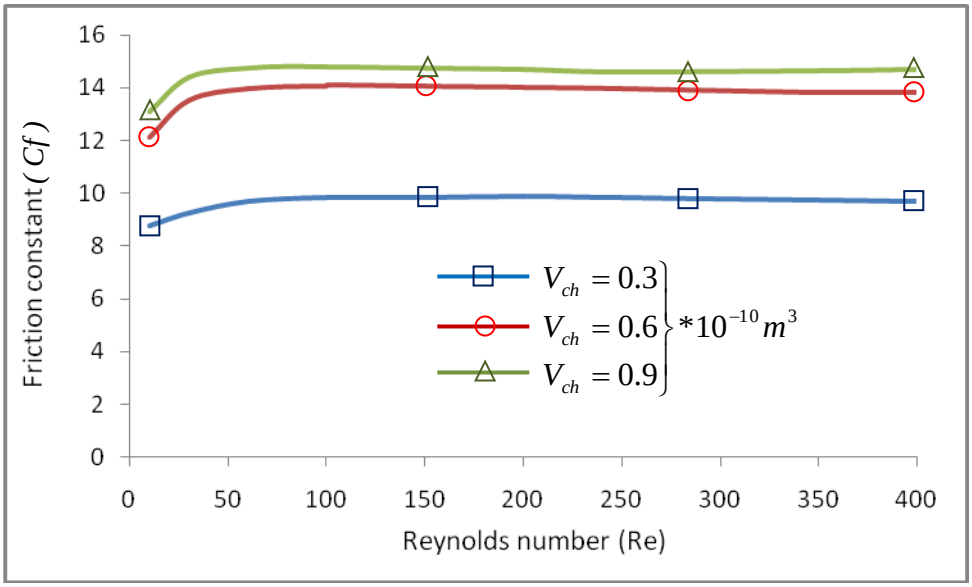

Fig.15. Variation of friction constant with Reynolds number for different channel volumes.

Figs. 16-18 indicate the variation of pressure drop, friction factor f and friction constant Cf with hydraulic diameter D_h for all Reynolds number, the pressure drop decreases with increasing D_h this due to the velocity of fluid inters the channels decreases. But both the f and Cf increases with increasing D_h this due to decrease the fluid flow in the channels and then the fluid friction increase. Both f and Cf will be similar behavior at Re=100 so they reduced from Figs. 17 and 18.

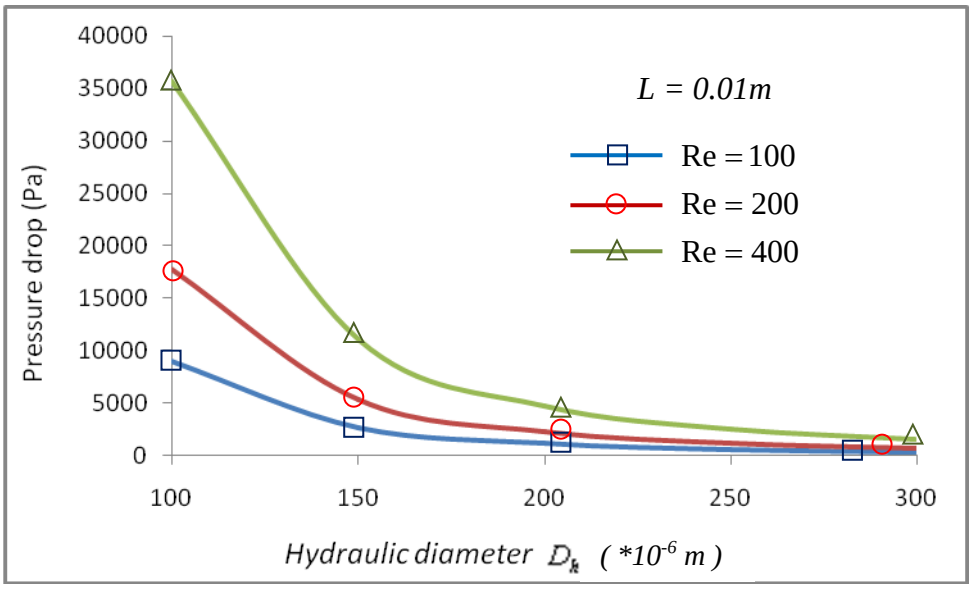

Fig.16. Variation of pressure drop with hydraulic diameter for different Reynolds number.

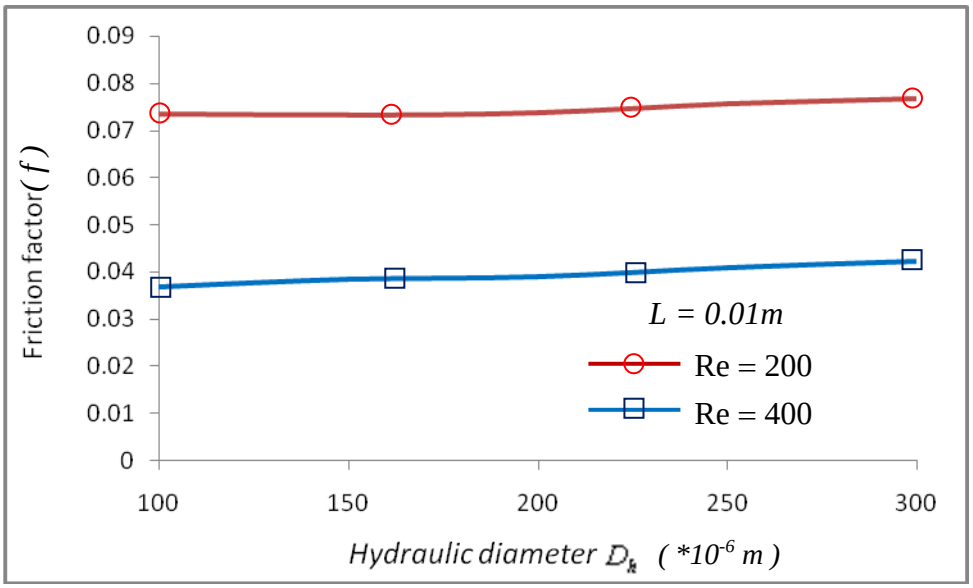

Fig.17. Variation of friction factor with hydraulic diameter for different Reynolds number.

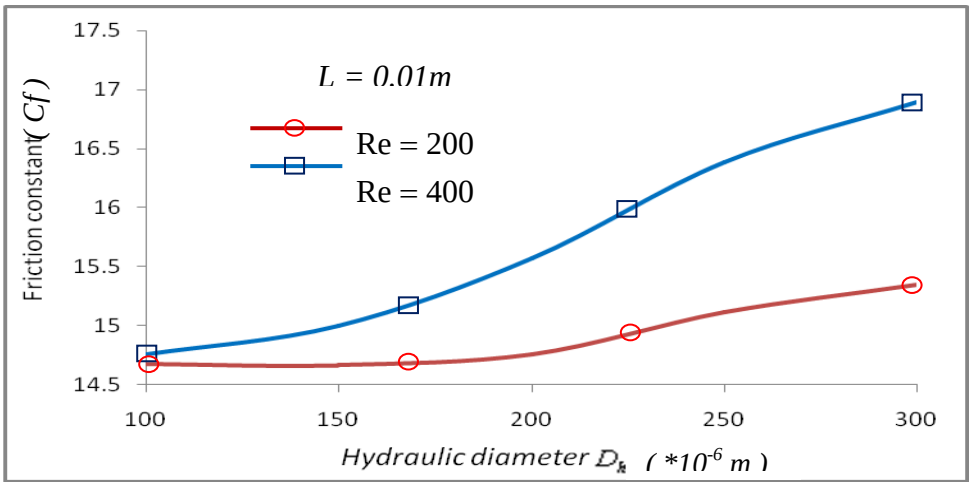

Fig.18. Variation of friction constant with hydraulic diameter for different Reynolds number.

For validity of present numerical results a comparison is made as shown in Fig. 19 for dimensionless centerline velocity $u^* = u/u_{in}$ in fully developed region against aspect ratio α between the results of present model and the analytical results of Shah and London [5]. The Fig. shows that the u^* increases with α and the present results give a good agreement. Another comparison between the present results and numerical results of Curr et al. [15] for the friction constant Cf against the dimensionless axial distance $x^+ = x/\sqrt{A}\,Re_{\sqrt{A}}$ where Re is based on square root of the flow area $\sqrt{A}$ instead the hydraulic diameter D_h as shown in Fig. 20 which indicates the Cf for both results is high at entrance region and decrease toward fully developed region and results difference seems acceptable.

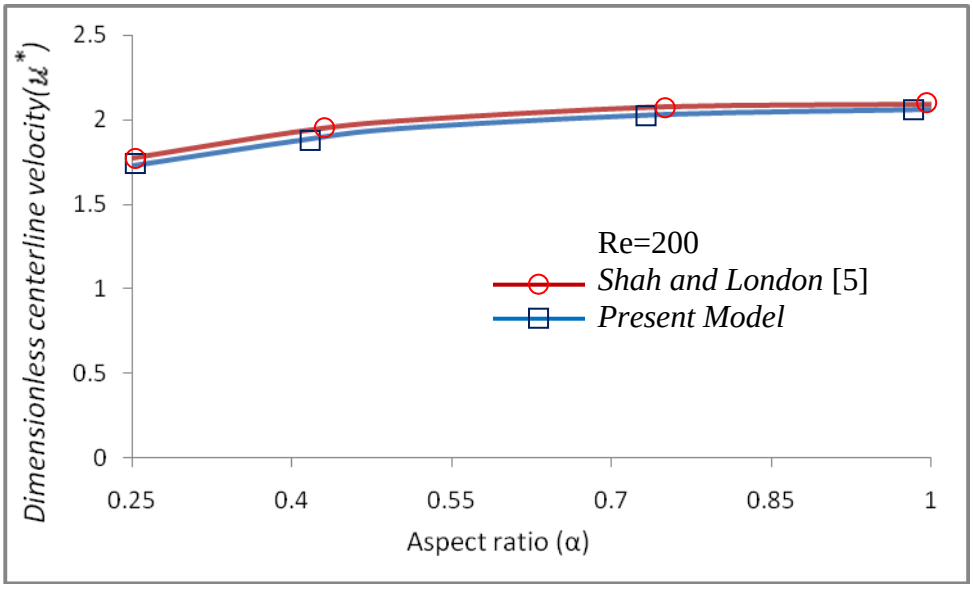

Fig.19. Comparison of dimensionless centreline velocity varied against aspect ratio.

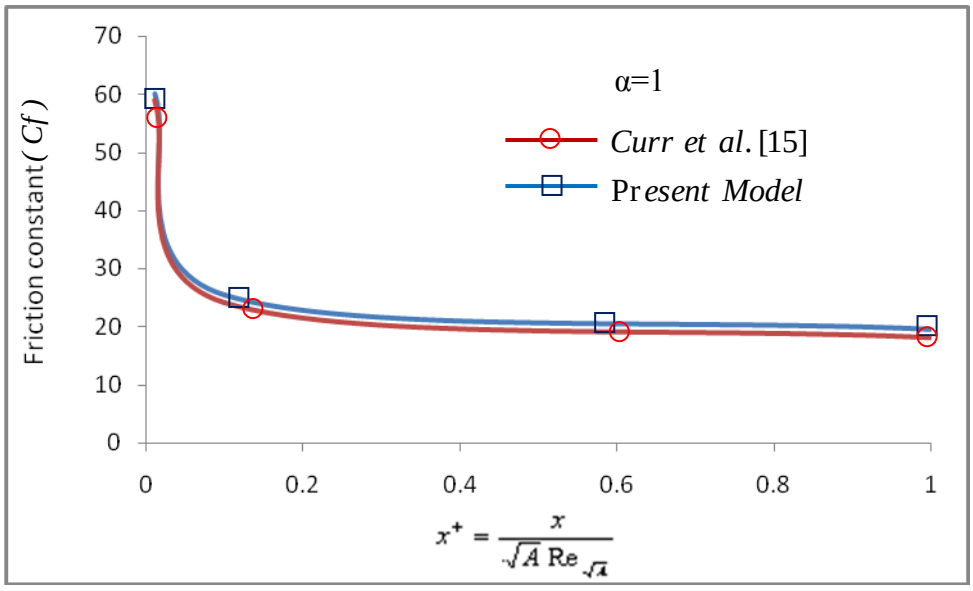

Fig.20. Comparison of friction constant varied against dimensionless axial distance.

5. Conclusions

Numerical simulation have been used to investigate the effects of the parameters: channel length L, Reynolds number Re, aspect ratio α, channel volume V_{ch} and hydraulic diameter D_h on pressure drop, friction factor f and friction constant Cf in three dimensional laminar flow of water in rectangular micro-channels. The continuity and Navier–Stokes equations are solved in the domain under concentration using the finite volume method with FORTRAN code. However, from the results obtained can be concluding that the pressure drop increase with increasing of L and Re, and decrease with increasing of α, V_{ch} and D_h each separately. On other hand, the f and Cf both increase with increasing of α, V_{ch}, D_h and L each separately and f alone decrease with increasing of Re. While Cf increase with increasing of Re, but less than Re=50 and then nearby with approximately constant value.

References

[1] R. Mahajan, R. Nair, V. Wakharkar, J. Swan, J. Tang and G. Vandentop, "Emerging Directions for Packaging Technologies", Intel Technology Journal, Q2 (06), 2002.

[2] M. Niklas, M. Favre-Marinet and D. Asendrych, "Numerical Simulation of Microchannel Network with Complex Geometry", Bulletin of The Polish Academy of Sciences, Technical Sciences, Vol. 53, No. 4, 2005.

[3] Amit S. Kulkarni, "Effects of Surface Roughness in Microchannel Flows", MSc Thesis, University of Florida, 2004.

[4] P. Wu and W. A. Little, "Measurement of Friction Factor for the Flow of Gases in Very Fine Channels Used for Micro-miniature Joule-Thomson Refrigerators", Cryogenics 23, pp. 273-277, 1983.

[5] R. K. Shah and A. L. London, "Laminar Flow Forced Convection in Ducts", Advanced Heat Transfer Suppl. 1, 1978.

[6] Yuri Stephan Muzychka, "Analytical and Experimental Study of Fluid Friction and Heat Transfer in Low Reynolds Number Flow Heat Exchangers", PhD Thesis, Waterloo, Ontario, Canada, (1999).

[7] J. Harley and H. Bau, "Fluid Flow in Micron and Submicron Size Channels", IEEE Trans., THO249-3, pp. 25-28, 1989.

[8] T. M. Adams , Abdel-Khalik, S. I. Jeter, S. M. Qureshi and Z. H., "An Experimental Investigation of Single-phase Forced Convection in Micro-channels", International Journal of Heat and Mass Transfer, Vol. 41, pp. 851-857, 1988.

[9] X. F. Peng and G. P. Peterson, "Convective Heat Transfer and Flow Friction for Water Flow in Micro-channel Structures", International Journal of Heat and Mass Transfer, Vol. 39, pp. 2599-2608, 1996.

[10] G. M. Mala and D. Li, "Flow Characteristics of Water in Micro-tubes", International Journal of Heat and Mass Transfer, Vol. 20, pp. 142-148, 1999.

[11] Mushtaq I. Hasan, "Numerical Simulation of Counter Flow Microchannel Heat Exchanger with Different Channel Geometries and Working Fluid", PhD Thesis, Mechanical Engineering Department, Collage of Engineering, Basrah University, 2009.

[12] Hayder M. Hasan, " Numerical Simulation of Parallel Flow Microchannel Heat Exchanger with Isosceles Right Triangular Geometry", MSc Thesis, Mechanical Engineering Department, Collage of Engineering, Basrah University, 2009.

[13] Merle C. Potter and John F. Foss, "Fluid Mechanics", Great Lakes Press, INC. Okemos, MI 48864, 1982.

[14] H. K. Versteeg and W. Malalasekera, "An introduction to Computational Fluid Dynamics-The Finite-Volume Method", Longman, 1995.

[15] R. M. Curr, D. Sharma and D. G. Tachell "Numerical Predictions of Some Three Dimensional Boundary Layers in Ducts", Computer Methods in Applied Mechanics and Engineering, Vol. 1, pp. 143-158, 1972.